A MICROMECHANICAL ULTRASONIC DISTANCE SENSOR WITH >1 METER RANGE

Richard Przybyla[1], Anita Flynn[1], Vipul Jain[1], Stefon Shelton[2], André Guedes[2], Igor Izyumin[1], David Horsley[2], and Bernhard Boser[1]*
Berkeley Sensor and Actuator Center
[1]University of California, Berkeley, CA, USA
[2]University of California, Davis, CA, USA

ABSTRACT

Ultrasonic distance sensors based on piezoceramic transducers have >1m range and millimeter accuracy but require the use of bulky transducers. Existing micromachined sensors deliver inferior performance, with maximum range in the tens of centimeters. We present theory, design equations, and measured results for a micromechanical ultrasonic distance sensor which approaches the performance of piezoceramic-based solutions. The sensor has a maximum range >1300mm and random errors (3σ) of <1.7mm at 1.3m.

KEYWORDS

Ultrasound transducer, piezoelectric, micromachined, aluminum nitride, time-of-flight, distance sensor

INTRODUCTION

Ultrasonic distance measurement is an attractive alternative to systems which rely on the speed of light, since the speed of sound is 6 orders of magnitude slower than the speed of light. However, ultrasonic systems that use bulk piezoceramics do not take full advantage of the power savings that come from operating at relatively low frequency, because of the large parasitics and low efficiencies of the piezoceramic transducers.

Capacitive [1] and piezoelectric [2] micromachined ultrasound transducers (cMUTs and pMUTs) mitigate this problem by using integrated circuit technology to build thin, flexible membranes that couple directly to the air. pMUTs are capable of a larger linear displacement range than cMUTs since the piezoelectric effect is inherently linear. This large displacement range is critical in air, since air's low acoustic impedance limits the maximum output power. Air-coupled cMUTs require bias voltages of hundreds of volts [1].

In this work, we present the design of an ultrasonic distance sensor with a maximum range of >1.3m which measures the distance between two identical aluminum nitride (AlN) pMUTs. We derive analytical expressions for the signal-to-noise ratio and the random distance error, and use these determine how transducer parameters and material properties affect the performance of the system. Experimental data matches the theory well.

ULTRASOUND TRANSDUCER

The ultrasound transducer [3] is a circular piezoelectric unimorph membrane which is released with a backside through-silicon etch. As shown schematically in Figure 1, electric field between the Au top electrode and the Pt bottom electrode creates a transverse stress in the 1µm thick AlN piezoelectric layer due to the inverse piezoelectric effect. The 1µm thick passive SiO_2 layer causes a vertical stress gradient which forces the membrane to deflect vertically, creating a pressure wave. Similarly, an incident pressure wave creates a force on the membrane and causes charge to develop between the electrodes.

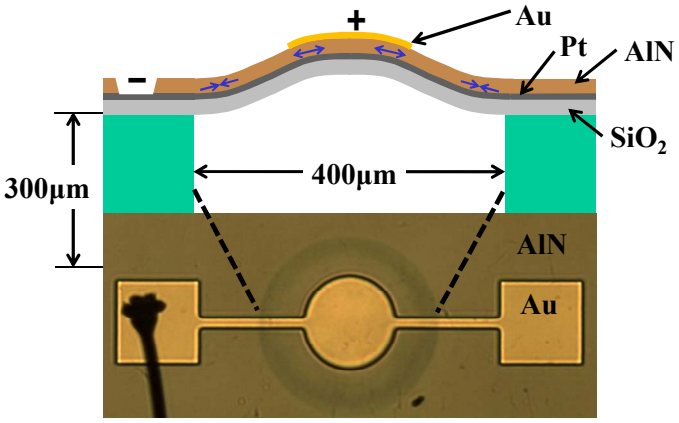

Figure 1: Schematic cross-section of pMUT and optical micrograph of pMUT. The AlN and SiO_2 layers are 1µm thick. The cross-section shows the bending mode that results when voltage is applied between the top and bottom electrodes.

The nominal resonant frequency of the transducer f_o is 215kHz, and the radius of the membrane is 200µm. The dynamics of the membrane are dominated by the stiffness and the mass of the membrane itself, yielding a quality factor Q of 20, resulting in a typical bandwidth of $f_o/(2Q)$ = 5.4kHz. The electrical impedance of the pMUT is dominated by the parallel-plate capacitance of the device (4 pF) and the bond pads (10 pF). Improved interconnect can reduce the total capacitance to ~5 pF. At resonance, the motional impedance of the device is 450kΩ, and the mechanical efficiency is approximately 15%. A model for the electrical, mechanical, and acoustical behavior of the device that was presented in [4] forms the basis for design of the distance sensor system.

SYSTEM DESIGN

The intended application of the sensor requires a high sampling rate, a maximum range of greater than 1 meter, millimeter accuracy, and minimum power and complexity.

To meet the sampling rate and complexity constraints, the system should produce a distance estimate

This material is based upon work supported by the Defense Advanced Research Projects Agency (DARPA) and/or the Space and Naval Warfare Center, San Diego (SPAWAR SSC-SD) under Contract No. N66001-08-C-2023.
*Corresponding author: rjp@berkeley.edu

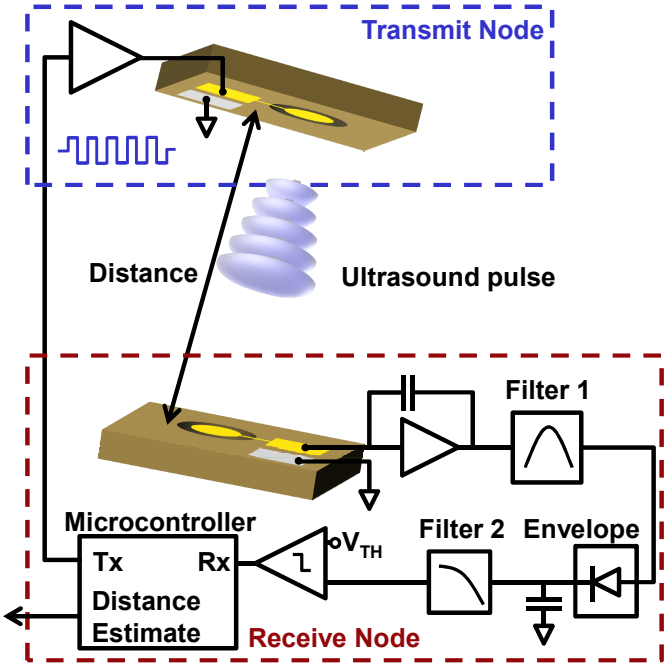

Figure 2: Distance Sensor Block Diagram

for each pulse it transmits. The system should also produce the distance estimate in a way that does not require complicated digital signal processing. This precludes matched filtering, which is the optimal detection algorithm [5] but requires correlation of the transmit waveform with the received waveform. Instead, simple threshold detection determines the arrival time of the pulse.

The resulting system block diagram is shown in Figure 2. The system is controlled by a microcontroller, which creates a burst at the resonant frequency of the device. The burst is sent electrically to the transmit node, which amplifies the signal and applies it to the transmit pMUT, which creates an output pressure wave. The signal propagates to the receive node acoustically, and the receive pMUT converts the input pressure to a voltage. The front-end charge amplifier produces an output proportional to the receive membrane displacement. After filtering out-of-band noise from the amplifier, the envelope is detected and compared to the detection threshold. The microcontroller measures the delay T_D between the transmit pulse and the received pulse. The distance estimate $D = cT_D$ is inferred from the speed of sound c.

For this system, the important design considerations are the transmit amplitude, transmit pulse shape, and the bandwidth of the receiver. These affect the maximum range and the distance error due to random noise.

The transmit amplitude is reduced by the nonlinearity of the transmit pMUT, which results in gradual gain compression when the input amplitude is above 1V. The transmit power is dominated by the CV^2f power required to drive the transducer capacitance, and the nonlinearity results in reduced efficiency at high transmit amplitudes. As a result, ultra low power systems requiring modest performance may choose to limit the transmit voltage. In this system, the transmit voltage was maximized to increase performance. Practical details limited the output voltage amplitude to 13V.

The maximum range of the sensor is determined by the minimum signal-to-noise ratio (SNR) required to reliably detect the received pulse and to reject false-alarms due to noise. The dominant noise sources in the system are the receive transducer and the front-end amplifier, discussed in more detail in the next section.

The design of the pulse shape is limited by the transducer characteristics. The narrowband nature of the transducer requires that $\sim Q$ cycles are transmitted at the resonant frequency for the transducer to ring-up to full amplitude. If additional range is required, the duration of the transmit pulse can be increased, and the bandwidth of the bandpass filter following the front-end can be decreased, reducing the noise variance and thereby extending the range. However, as discussed next, this degrades the distance noise performance of the system.

For a time-of-flight based system, distance noise is created when amplitude noise is converted to timing noise by the finite rise time of the transmit pulse. Therefore, the ideal transmit waveform has zero rise time. Since any real system is band-limited, the bandwidth of the system limits the maximum achievable noise performance. The rms distance error σ_d for a linear detector is given by [5]:

$$\sigma_D = c\frac{\sigma_A}{\beta S}, \qquad (1)$$

where σ_A is the rms amplitude noise, β is the effective bandwidth, and S is the amplitude of the signal. Since the amplitude noise variance σ_A^2 is proportional to the bandwidth, the distance noise variance σ_D^2 decreases linearly as the bandwidth increases. For this reason, the optimal noise performance is achieved when the bandwidths of the transmit pulse, the transmitter, and the receiver are greater than the transducer bandwidth, so that the bandwidth of the signal is limited by the transducer only.

MAXIMUM RANGE

Figure 3 shows an equivalent circuit model for the receive pMUT and the front-end amplifer. At resonance, the transmitter's acoustic output is 256Pa at the Rayleigh range. The ultrasonic channel attenuates the signal due to spreading and absorption loss [6]:

$$G_{ch} = \frac{p_{rx}}{p_{tx}} = G_{ac}\frac{r}{2D}10^{-\alpha D}, \qquad (2)$$

where G_{ac} is the acoustic gain, r is the effective membrane radius, and α is the attenuation coefficient, measured as 7dB/m at 215kHz and at room temperature and 60% relative humidity. The acoustic gain is 1 for the front side of the membrane, and approximately 21 for the back side. This gain is caused by the large hole in the printed circuit board that exposes the backside of the membrane to the air, thereby increasing the effective area of the transducer, and also making it more directional. For

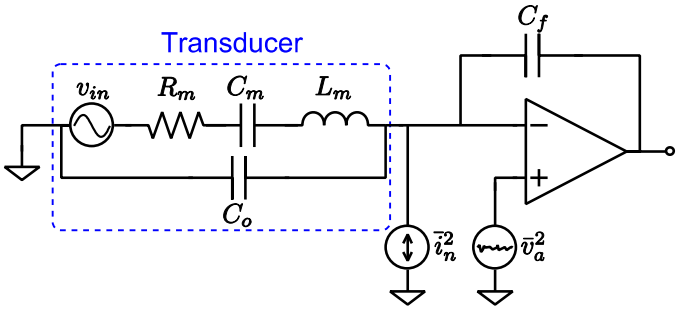

Figure 3: Electrical model for transducer and front-end amplifier showing relevant noise sources

the transmitter, $p_{tx} = V_{tx}\gamma\eta/\mathrm{SA}$, where SA is the effective surface area of the membrane, η is the voltage-to-force coupling factor, and γ is the mechanical efficiency which includes the transducer nonlinearity.

An incident pressure wave creates a force on the receiver's membrane, which is converted to a voltage by the piezoelectric effect. The output from the integrator is:

$$v_o = \frac{p_{rx}\mathrm{SA}}{\eta Z_m} Z_{C_f}, \tag{3}$$

where Z_{C_f} is the impedance of the feedback capacitor, and Z_m is the series impedance of the pMUT, equal to R_m at resonance. SA/η is equal to 5.9mV/Pa.

The pMUT's motional resistance R_m models the mechanical damping of the membrane, which results from air damping and substrate loss. The amplifier is biased by a large feedback resistor ($\gg R_m$). Because of the pMUT's high impedance, MOS input devices yield minimum noise. The amplifier's voltage noise is amplified due to capacitor C_o' which includes the transducer capacitance and the amplifier input capacitance. The resulting output noise density is

$$\frac{\bar{v}_{o,a}^2}{\Delta f} \cong \bar{v}_a^2 \left(\frac{Z_{C_f}}{Z_{C_o'}}\right)^2 + Z_{C_f}^2 \frac{4kTR_m}{Z_m^2}, \tag{4}$$

where Z_{C_f} and $Z_{C_o'}$ are the impedances of the feedback capacitor and the parasitic capacitance, and $C_o' \gg C_f$. As mentioned before, the bandpass filter that follows the front-end should have a larger bandwidth than the transducer. As a result, the electronic noise is filtered by the bandpass filter, but the mechanical noise is filtered by Z_m, with noise bandwidth $\sim R_m/(4L_m)$. The filter's output noise variance is

$$\bar{v}_{o,f}^2 \cong \mathrm{G_f^2} Z_{C_f}^2 \left(\bar{v}_a^2 (\omega_o C_o')^2 \mathrm{NBW_f} + \frac{kT}{L_m}\right), \tag{5}$$

where $\mathrm{G_f}$ is the filter gain and $\mathrm{NBW_f}$ is the filter bandwidth. Using $R_m = b_m/\eta^2$, $L_m = m_m/\eta^2$, (2), (3), and (5), the SNR for the system at resonance is

$$\mathrm{SNR} \cong \frac{\left(\frac{\eta\gamma}{b_m} V_{tx} \mathrm{G_{ch}}\right)^2}{\left(\bar{v}_a^2 \frac{k_m C_o'^2}{m_m \eta^2} \mathrm{NBW_f} + \frac{kT}{m_m}\right)}, \tag{6}$$

where m_m, k_m, and b_m are the mass, stiffness, and damping of the membrane.

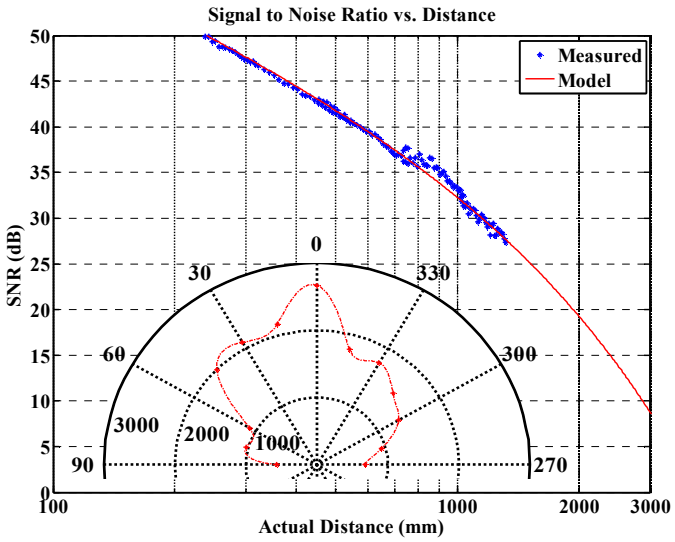

Figure 4: Signal-to-noise ratio vs. distance, measured and model. Inset: maximum range (mm) vs. angle.

Eq. (6) shows that the electromechanical coupling factor η is critical for performance. In our system, the electronic noise is nearly equal to the mechanical noise. If mechanical noise dominates, the SNR is proportional to η^2, but if electronic noise dominates, it is proportional to η^4. Also, when electronic noise dominates, the ratio η^2/C_o' is critical for performance. If C_o' is dominated by the device parasitic, then η^2/C_o' is proportional to $e_{31}^2/\varepsilon_{33}$, where e_{31} is the piezoelectric constant and the ε_{33} is the dielectric constant of the material. Using this metric, AlN compares favorably to PZT because of AlN's drastically reduced dielectric constant. The value of $e_{31}^2/\varepsilon_{33}$ is 10.6GPa for AlN and 9.4GPa for PZT [7].

The maximum range is based on the maximum error rate. The threshold must be set high enough to prevent false alarms, but low enough to reliably detect the signal at the maximum range. The average time between false alarms is given in [5]:

$$\mathrm{t_{fa}} = \frac{1}{\mathrm{BW}} \mathrm{e}^{\mathrm{V_{TH}^2}/\sigma_\mathrm{A}^2}, \tag{7}$$

which results in $\mathrm{V_{TH}^2}/\sigma_\mathrm{A}^2$=12dB for $\mathrm{t_{fa}}$ =30 minutes. Because of the exponent in (7), $\mathrm{t_{fa}}$ is very sensitive to $\mathrm{V_{TH}^2}/\sigma_\mathrm{A}^2$; reducing the margin to 11dB results in $\mathrm{t_{fa}}$=54 sec. Using $\mathrm{t_{fa}}$ =30 minutes, the theoretical maximum range occurs when (6) is equal to 12dB. Figure 4 shows the theoretical SNR vs. distance. The theoretical maximum range is 2.6 meters. The measured data matches the theoretical SNR well. Limitations in the test setup prevented measurements over 1.3m.

DISTANCE ERROR SOURCES

Distance measurement errors result from systematic errors and random errors. Systematic errors mainly come from environmental factors and fixed (i.e. offset and gain) errors from the receive circuit. The error due to the variation of the speed of sound with temperature is 1.75mm/m/℃. As a result, to reduce systematic error to less than the theoretical random error floor, a

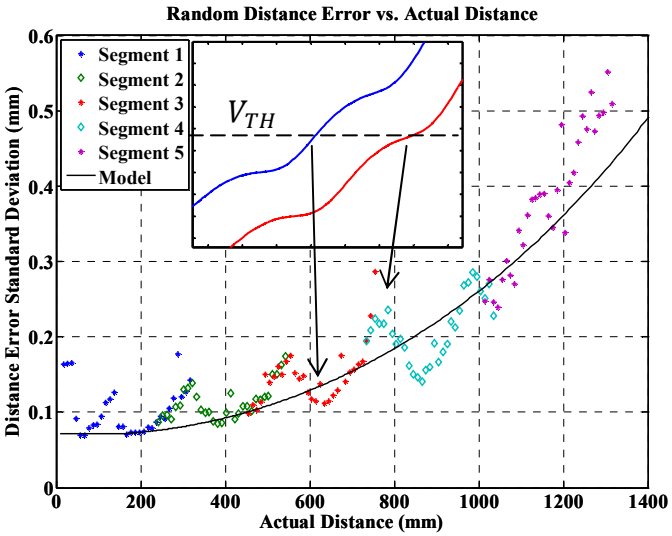

Figure 5: Random distance error vs. actual distance, measured and model. Inset: Envelope signal, showing how ripple (exaggerated) at f_o *modulates the distance noise.*

thermometer with an accuracy of 0.1 °C is needed. Alternatively, a ratiometric measurement can be made, where the ultrasonic delay T_D is compared to the delay from a second reference path which has a known distance.

The finite rise time of the pulse also leads to a systematic gain error, since the time between the beginning of the receive pulse and the crossing of the threshold depends on the amplitude of the pulse. This can be calibrated out, or eliminated by referencing the threshold to the pulse amplitude.

Random errors arise from noise in the receive transducer and the front-end amplifier. Using (6), we can re-write (1) in terms of the transducer parameters:

$$\sigma_D^2 = c^2 \frac{m_m \left(\bar{v}_a^2 \frac{k_m C_o'^2}{\eta^2} \mathrm{NBW_f} + kT \right)}{\left(\frac{\kappa}{2} \eta \gamma V_{tx} \mathrm{G_{ch}} \right)^2}, \qquad (8)$$

where we have used $\kappa b_m/m_m$ as the effective bandwidth of the system, and where κ is a scaling constant dependent on the pulse shape [5], measured to be 0.34 for our system. Interestingly, increasing m_m increases the SNR (and the maximum range) but also increases the distance noise.

Eq. (8) also yields insight about device scaling. Since $m_m \propto r^2 h$, $k_m \propto h^3$, $b_m \propto r^2$, $\eta \propto 1/h$, $\mathrm{C_o} \propto r^2/h$, $\mathrm{NBW_f} \propto b_m/m_m$ and $\gamma \propto h$, where h is the thickness of the membrane [3], systems dominated by electronic noise will have $\sigma_D \propto r^2 h^{3/2}$ for C_o' dominated by transducer parasitic and $\sigma_D \propto h^{5/2}$ for C_o' dominated by amplifier parasitic. Systems dominated by mechanical noise will have $\sigma_D \propto \sqrt{h}$. In either case, (8) suggests that decreasing the device thickness would further increase performance.

MEASUREMENT RESULTS

Figure 5 shows the random distance error vs. distance for the system. At short distances, the random error is dominated by the finite timing resolution of the system. As shown in Figure 5, the periodic structure in the random error is due to ripple at f_o that remains after the peak detector and second lowpass filter. The residual ripple modulates the input to the threshold detector. The noise is increased when the ripple reduces the slope of the pulse envelope, and decreased when the ripple increases the slope. This could be suppressed with a higher-order filter at the output of the peak detector, or by referencing the threshold to the pulse amplitude as mentioned previously.

CONCLUSION

Aluminum nitride piezoelectric micromachined ultrasound transducers enable practical distance measurement over the range of several meters, with sub-mm accuracy. Expressions for the signal-to-noise ratio and the random distance error show that there is a tradeoff between the maximum range and the random distance error, and that if the device dimensions are scaled down, the distance accuracy improves. If the system is limited by noise from the electronic circuitry, the maximum range and accuracy of the system are maximized when the figure of merit $e_{31}^2/\varepsilon_{33}$ is maximized. AlN compares favorably to other piezoelectrics when using this figure of merit.

ACKNOWLEDGEMENT

Simone Gambini provided helpful advice.

REFERENCES

[1] I. Wygant *et al.*, "50 kHz capacitive micromachined ultrasonic transducers for generation of highly directional sound with parametric arrays," *IEEE Trans. Ultrason., Ferroelectr., Freq. Control,* vol. 56, no. 1, pp. 193–203, Jan. 2009.

[2] P. Muralt *et al.*, "Piezoelectric micromachined ultrasonic transducers based on PZT thin films," *IEEE Trans. Ultrason., Ferroelectr., Freq. Control*, vol. 52, no. 12, pp. 2276–2288, Dec. 2005.

[3] S. Shelton *et al.*, "CMOS-compatible AlN piezoelectric micro- machined ultrasonic transducers," in *Proc. IEEE Ultrasonics Symp. 2009*, Oct. 2009, pp. 402–405.

[4] R. Przybyla *et al.*, "An ultrasonic rangefinder based on an AlN piezoelectric micromachined ultrasound transducer," in *Proc. IEEE Sensors 2010*, Nov. 2010, pp. 2417–2421.

[5] M. Skolnik, *Introduction to Radar Systems*. 3rd edition, McGraw-Hill, 2001.

[6] D. Blackstock, *Fundamentals of Physical Acoustics*. John Wiley & Sons, 2000.

[7] P. Muralt, "PZT thin films for microsensors and actuators: Where do we stand?," *IEEE Trans. Ultrason., Ferroelectr., Freq. Control*, vol. 47, pp.903-915, July 2000.